IGC Newsletter

ISSN 0972-5741 Volume 137, Issue 3, July 2023

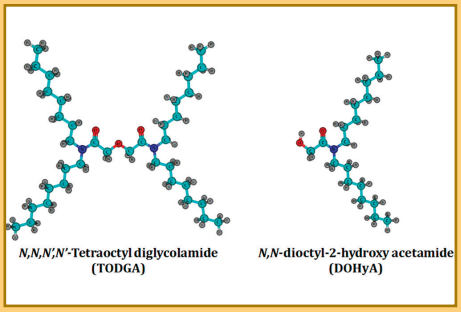

Director's Message

Dear Colleagues,

FBTR is in continuous operation in the 32nd irradiation campaign at the design target power of 40 MWt/10MWe. The total electrical energy developed in June 2023 is about 6.02 million units. An advanced computer simulation code has been developed in-house for the prediction of distribution ratio of actinides and fission product concentration profiles in the presence of degradation products in process streams of fuel reprocessing. In KAMINI, trail run for real-time neutron radiography using camera with un-irradiated plastic based material in south beam tube location up to 20kW power level was conducted.

A Met-Ocean Data Buoy with meteorological, ocean sensors and Environmental Radiation Monitor (ERM) has been installed off Kalpakkam site. The buoy provides crucial radiation field input from the ocean sector for the Online Emergency Decision Support System. It also provides data on currents for radioactivity dispersion, wave height and weather parameters during extreme weather conditions for the purpose of early warning.

A collaborative incubation agreement, as per DAE Incubation Policy (2021), has been signed on 25 April 2023 between DAE Incubation Centre-IGCAR and a Chennai based private industry, M/s. KritiLabs Technologies Pvt. Ltd., for IGCAR's "Oil Level Measurement System".

A six-week summer Training Programme in Physics and Chemistry (STIPAC-23) for M.Sc., Physics and Chemistry students from various institutions is underway.

I appreciate the efforts of the editorial committee and the authors for their contributions to the newsletter.

[B. Venkatraman]
Director, IGCAR & GSO

Editor's Desk

Dear Reader

Greetings

It is my pleasant privilege to forward the latest issue of IGC Newsletter (Volume 137, July 2023, Issue 3). I thank my team for their timely inputs, cooperation, and support in bringing out this issue.

The technical article of this issue "Effects of Structural Variation of Glycolamide Extractants in the Treatment of High-level Waste Solutions" is by Dr. T. Prathibha and colleagues, MC&MFCG from MCMFG, IGCAR.

Young Officer's Forum features an article on "Preparation of 316L(N) stainless steel weld joints containing 0.05 to 0.14 wt.% N and study on its microstructure and properties" by Dr. M. Divya, MMG, IGCAR.

The article on "Development of Interlayer Coatings on Graphite with Top Y_2O_3 Coating for Pyrochemical Reprocessing Applications" by Dr. Madhura. B from MMG, IGCAR is categorised as this issue's Young Researcher article.

In the back cover, we have Red-Whiskered Bulbul a rarely spotted bird in Kalpakkam Complex.

The Editorial Committee would like to thank all the contributors. We look forward to receiving constructive suggestions from readers towards improving the IGC Newsletter content.

We express our deepest gratitude to Director IGCAR for his keen interest and guidance.

With best wishes and regards

S. Rajeswari
Chairman, Editorial Committee, IGC Newsletter and
Head, Scientific Information Resource Division, IGCAR

Effects of Structural Variation of Glycolamide Extractants in the Treatment of High-level Waste Solutions

The amide derivatives of diglycolic acid having long carbon chains, usually C_8 or higher, have attracted the interest of separation chemists working for nuclear waste management applications since last 2-3 decades. Commonly described as 'diglycolamides', these are tridentate ligands having two carbonyl groups on either side of an ethereal oxygen, capable of extracting trivalent actinides in high-level waste solutions. The separation of trivalent actinides, Am(III) and Cm(III) in high-level waste solutions is considered as an essential step before vitrification and final disposal of these waste in deep geological repositories. Long-lived alpha emitting radioisotopes of neptunium, americium and curium have been identified as the major contributors of decay heat and long-term radiotoxicity of nuclear waste after separation of plutonium and uranium during nuclear reprocessing. While neptunium is separated along with uranium and plutonium in advanced reprocessing cycles, americium and curium remain in the high-level waste solutions generated after reprocessing. Solvent extraction cycles employing diglycolamide based solvents have been found to be useful for the separation of these trivalent actinides from other fission products. The efficient separation processes using diglycolamide solvents for removal of trivalent actinides along with chemically similar lanthanides from genuine HLW solutions have been demonstrated in Germany and India.

Though diglycolamide solvents have good extraction properties, the stripping cycles for recovery of extracted metal ions from these solvent phases required the use of complexing agents in the stripping solution. Also, the high polar nature of diglycolamide ligands resulted in their extensive aggregation during metal ion extraction leading to the undesirable third phase splitting. A suitable phase modifier, usually a long chain alcohol, had to be used as a phase modifier along with diglycolamide ligands so as to avoid the third phase splitting. During recent studies in our group, a monoglycolamide ligand was identified as a better solvent having similar extraction properties as diglycolamide ligands. The stripping of extracted metal ions from monoglycolamide ligand was possible without the use of complexing agents and third phase splitting was prevented for this ligand due to its minimal aggregation. The structure of commonly used octyl derivative of diglycolamide ligand, N,N,N',N'-tetraoctyl diglycolamide (TODGA) and the corresponding monoglycolamide N,N-di-octyl-2-hydroxyacetamide (DOHyA) are shown in Figure 1. The consequences of structural variation of glycolamide ligands on various aspects such as aggregation behavior and complexation behavior during the extraction of trivalent metal ions were studied in detail by a comparison of TODGA and DOHyA ligands.

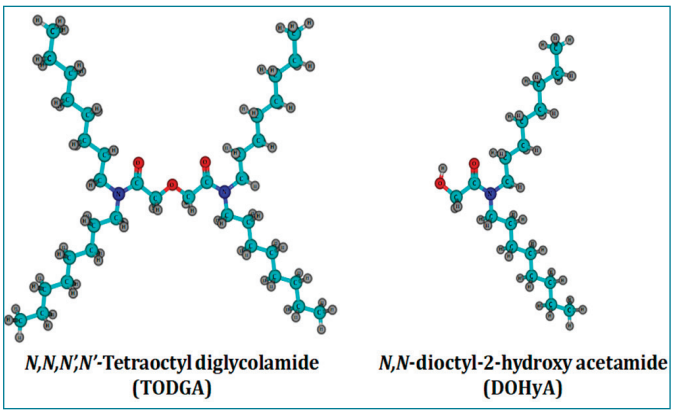

Figure 1: Structure of TODGA and DOHyA.

Aggregation Studies using Dynamic Light Scattering (DLS)

The dynamic light scattering technique is an effective tool for determination of the average aggregate sizes of reverse micellar aggregates formed by polar extractants during the extraction of metal ions from nitric acid solutions. The aggregation of extractants during solvent extraction and third phase splitting are the direct consequences of incompatibility of metal-extractant complexes in the non-polar diluents such as n-dodecane or NPH (Normal Paraffinic Hydrocarbon mixture) commonly employed for handling solutions of radioactive materials. The aggregation of TODGA with nitric acid is illustrated by the aggregate size distribution curves recorded for TODGA/n-dodecane solvent during extraction of nitric acid (Figure 2). The formation of reverse micellar aggregates of TODGA with nitric acid and metal ions was favoured by the increase in TODGA concentration as well as with increase in nitric acid /metal ion concentration of the aqueous phase. The bigger aggregates separated as a heavier organic phase in between the aqueous and organic phases. The presence of a phase modifier was always essential for TODGA for effective dispersion of such bigger aggregates during metal extraction.

Figure 3 compares the aggregate size distribution curves recorded for TODGA and DOHyA solvents equilibrated with 4 M nitric acid. The average aggregate sizes for DOHyA were much smaller in comparison with TODGA even at high extractant concentrations. The smaller aggregates of DOHyA were stable during metal ion extraction also, as they didn't show the tendency of phase splitting and allowed the extraction of stoichiometric quantities of metal ions. DOHyA formed smaller aggregates as a result of the lower polarity of the DOHyA molecule in comparison to TODGA. The high co-extraction of nitric acid in TODGA during metal ion extraction was another consequence of the high polarity of the molecule, leading

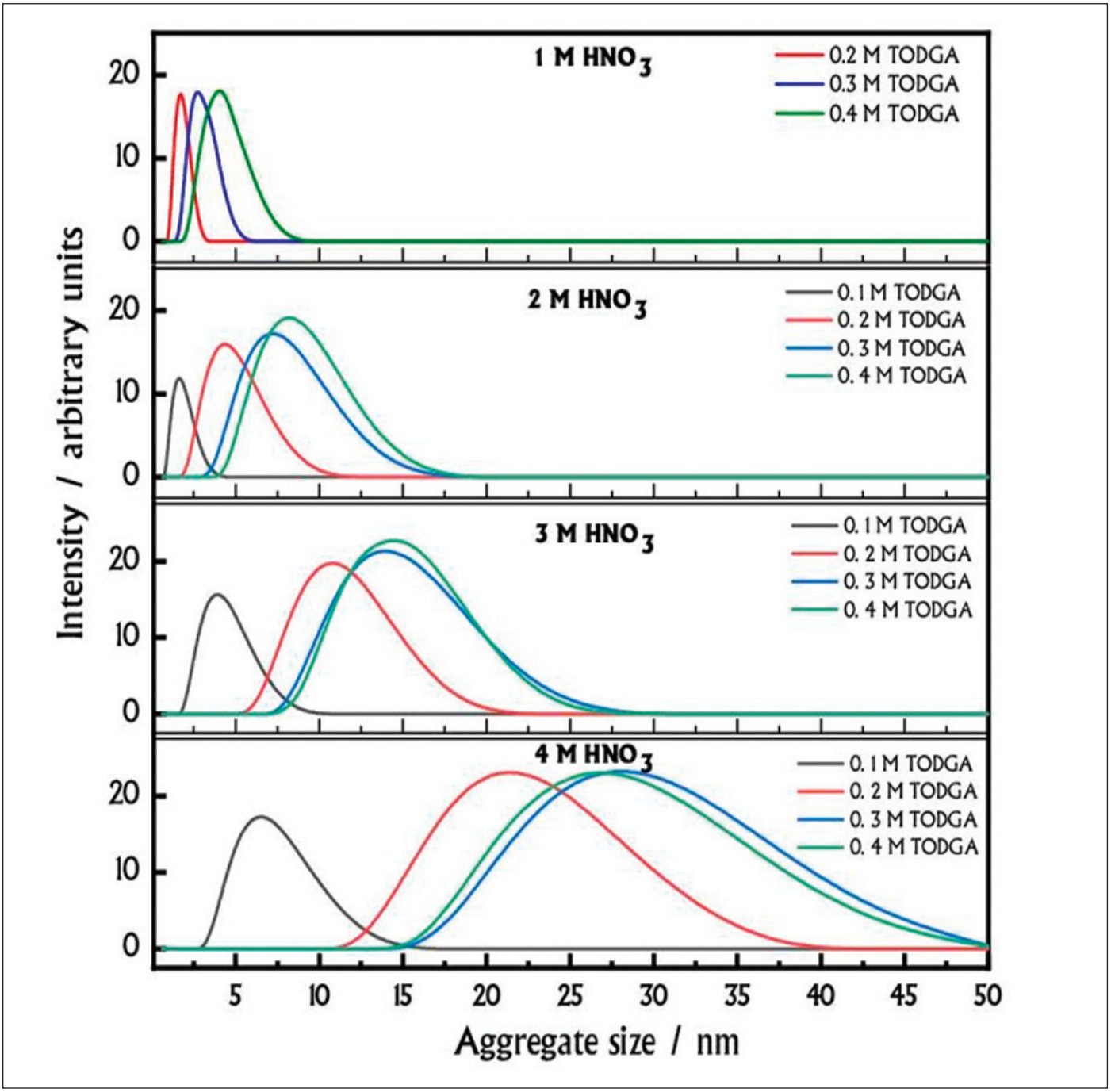

Figure 2: Aggregate size distribution curves for TODGA/n-dodecane solvent after equilibrating with nitric acid solutions

to problems in the back extraction of metal ions. DOHyA showed minimal co-extraction of nitric acid and hence the back extraction of metal ions was easier from DOHyA phase.

Electronic spectroscopy studies

The metal-ligand complexation during solvent extraction was studied by electronic spectroscopy involving UV-Visible and Time Resolved Luminescence Spectral (TRLS) analyzes. Figure 4 compares the UV-Vis absorption spectra of Nd(III) loaded organic phases containing TODGA and DOHyA in n-dodecane medium.

The spectra were recorded under similar loading of Nd(III) in both the solvents. TODGA solvent in n-dodecane contained 5 vol.% of 1-octanol so as to prevent third phase splitting. Figure 4 shows the variation in the intensity of hypersensitive peak of Nd(III) at 580 nm after complexation with TODGA and DOHyA. The peak intensities were found to be significantly reduced after complexation with TODGA, indicating considerable changes in the Nd(IIII) ion environment after complexation with TODGA. On the other hand, the peak intensities decreased to a smaller extent after complexation with DOHyA, indicating only minimal changes in the Nd(III)

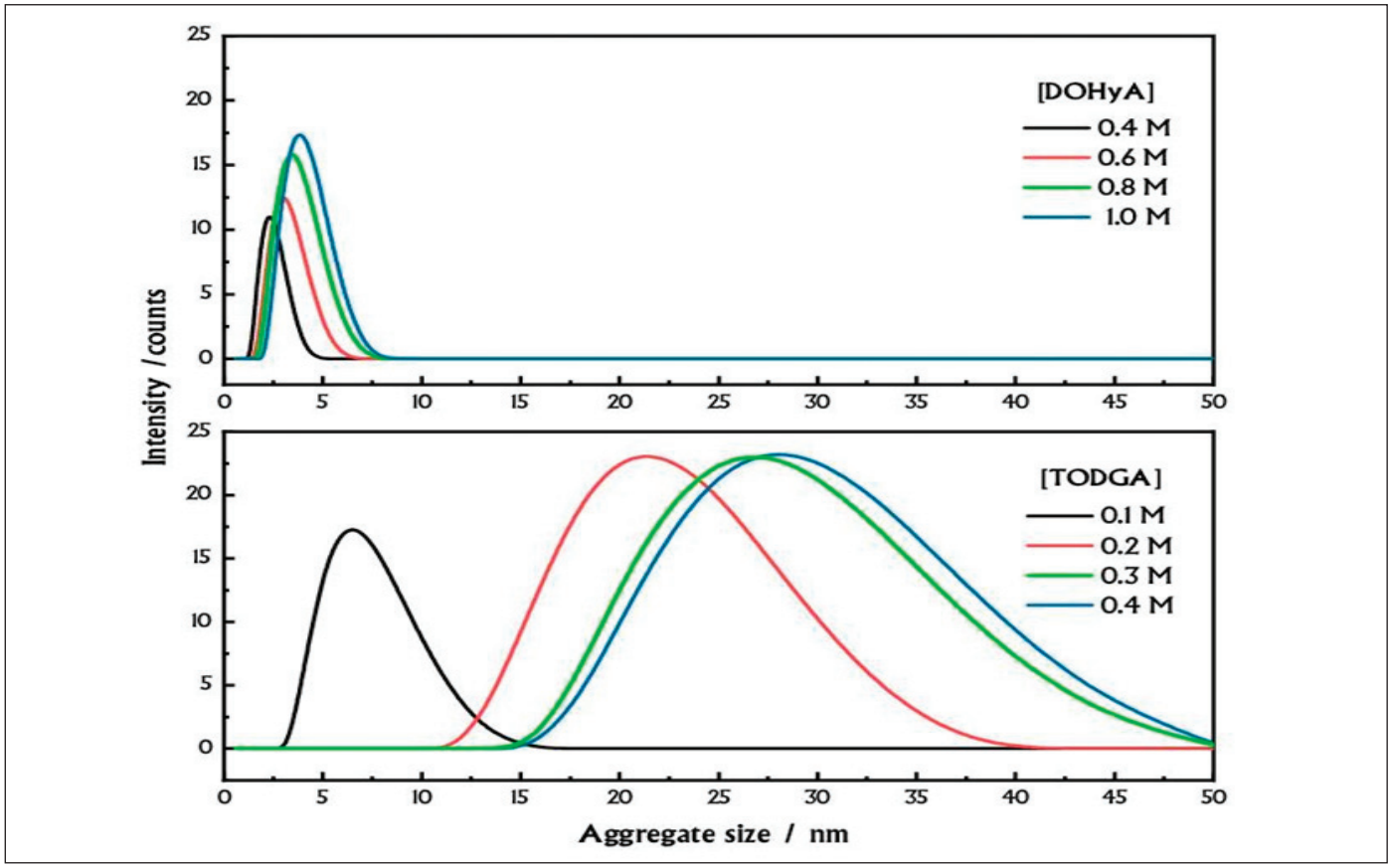

Figure 3: Comparison of aggregate distribution curves in DOHyA and TODGA solvents in n-dodecane after equilibration with 4 M nitric acid

environment in DOHyA phase. It was inferred that the metal ion environment is more stable and hydrophilic in the DOHyA phase, as compared to the TODGA phase. The complexation of trivalent metal ions by TODGA and DOHyA was further probed by luminescence spectroscopy. Here, Eu(III) was chosen as a model lanthanide ion due to its excellent luminescence properties. Table 1 compares the values of fluorescence life-time (decay constant) calculated for Eu(III) after complexation with both TODGA and DOHyA ligands in n-dodecane medium.

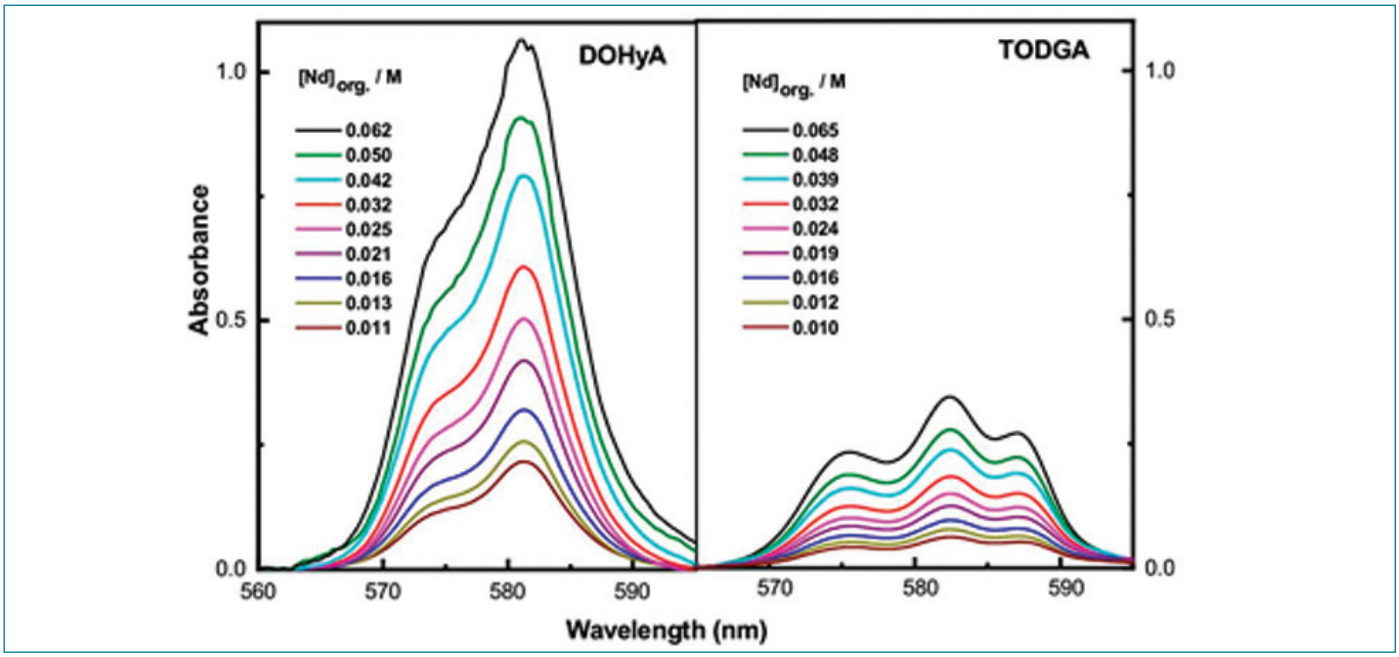

Figure 4: The UV-Vis absorption spectra of DOHyA and TODGA solvent phases at different loadings of Nd(III). Aqueous phase used for extraction: Nd(III) in 4 M nitric acid. Organic phase: 0.4 M DOHyA/n-dodecane or 0.2 M TODGA/n-dodecane + 5 vol% 1-octanol.

Enhanced co-extraction of water in H-bonding ligands during metal ior extraction improves the stability of solvent phase

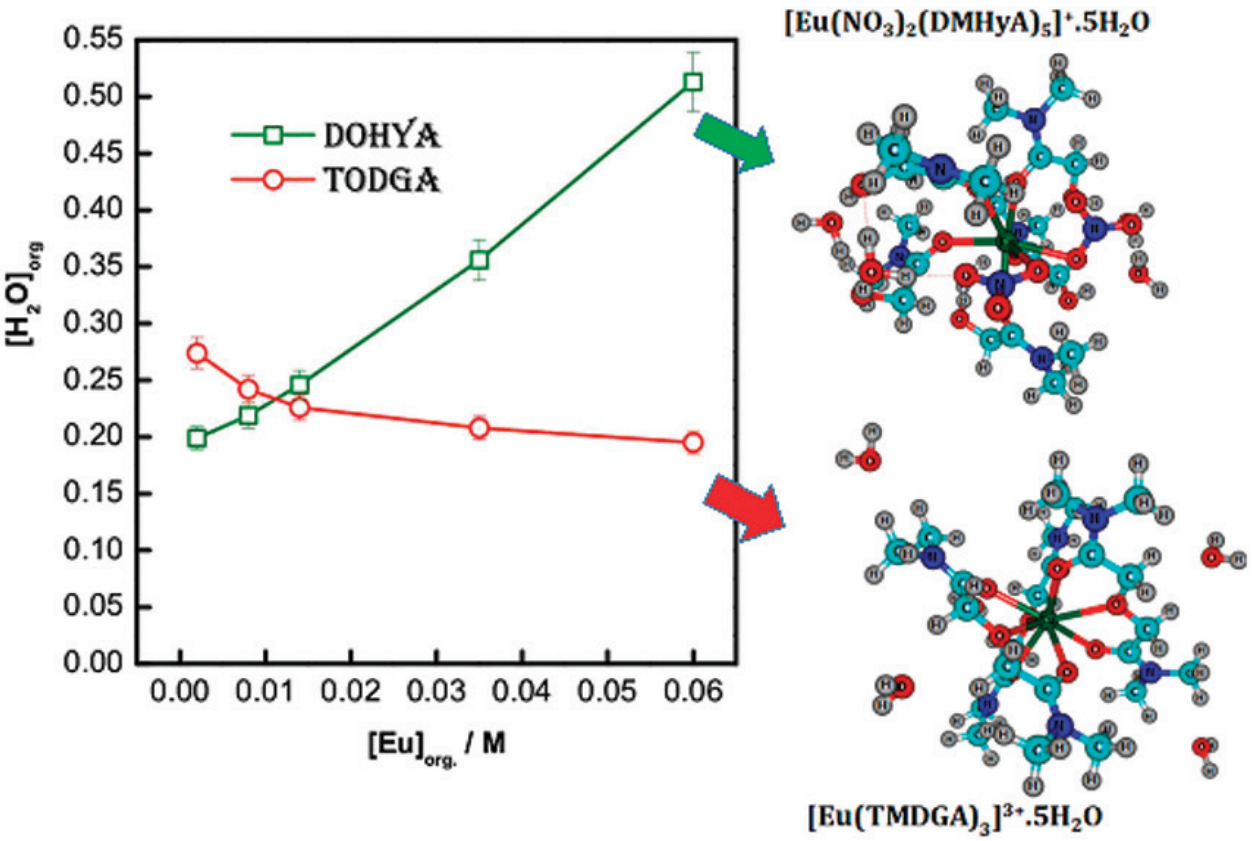

Figure 5: Co-extraction of water during the extraction of Eu(III) by TODGA and DOHyA solvent phases. Aqueous phase: Eu(III) in 4 M nitric acid. Organic phase: 0.4 M DOHyA/n-dodecane or 0.2 M TODGA/n-dodecane + 5 vol% 1-octanol

Table 1 Decay constants and NH_2O for TODGA and DOHyA at different concentrations of Eu(III) in the organic phase.

[Eu]org /M	Luminescence life-time / ms		NH_2O	
0.002	1.802	0.418	0	1.8
0.008	1.897	0.374	0	2.1
0.014	1.874	0.367	0	2.2
0.059	1.782	0.343	0	2.4

The decay constant values indicated the number of water molecules associated with Eu(III)-ligand complexes (NH2O). The results showed that TODGA complexes are devoid of water molecules in the complexes, while DOHyA complexes accommodated water molecules. This was further confirmed by determination of co-extracted water in TODGA and DOHyA solvent phases by Karl Fischer titration. The co-extraction of water by DOHyA was found to be more in comparison with TODGA. Figure 5 shows the amount of water measured for the solvent phases as a function of Eu(III) extraction. It was inferred that DOHyA-Metal complexes accommodated more water molecules, creating a better hydrophilic environment in the solvent phases during metal extraction. Probably, the hydroxyl group in the structure of DOHyA played a key role in the stabilization of water molecules around the metal clusters in solvent phase by hydrogen bonding. Figure 5 also shows the model structures of metal-ligand complexes of TMDGA and DMHyA optimized by Density Functional Theory (DFT) calculations.

Thus, the better compatibility of DOHyA-Eu complex in the non-polar diluent, n-dodecane could be attributed to the improved hydrophilicity of DOHyA due to the presence of hydroxyl groups in DOHyA molecule. The properties of the diglycolamide TODGA was tuned in an effective way by changing to the simpler monoglycolamide structure and the studies showed the promising nature of the monoglycolamide derivative, DOHyA for solvent extraction of trivalent metal ions.

Reported by
Dr. T. Prathibha and colleagues
MC&MFCG

Young Officer's Forum

Dr. M. Divya completed her B.E Metallurgical Engineering from G.C.E., Salem in the year 2007 and subsequently joined M.Tech. in Welding Technology at IIT Madras in the year 2007. She joined Materials Joining Section, MMG, IGCAR in the year 2008. She acquired Ph. D in the year 2020 from HBNI, IGCAR campus. Presently, she is working as Scientific Officer-E. Her research interests are welding metallurgy and weldability studies on steels, stainless steels and Ni base superalloys

Preparation of 316L(N) stainless steel weld joints containing 0.05 to 0.14 wt.% N and study on its microstructure and properties

Back ground

AISI 316L(N) austenitic stainless steel (SS) containing 0.07 wt.% nitrogen (N) is used as structural material for high temperature components operating in sodium environment of Prototype Fast Breeder Reactor (PFBR). Components of the reactor are fabricated by welding process either by using shielded metal arc welding (SMAW) or gas tungsten arc welding (GTAW) process based on its section thickness. AWS 5.4 E316-15M electrode containing ~0.07 wt.% N was developed to match the composition and strength of 316L(N) SS and used for fabrication of thick section reactor components using SMAW process. ER 16-8-2 consumable is preferred for Tungsten Inert Gas (TIG) welding process for welding 316L(N) SS as standard nitrogen containing filler wires are not commercially available. Future FBRs (Fast Breeder Reactor) are designed for a 60 years' service life.

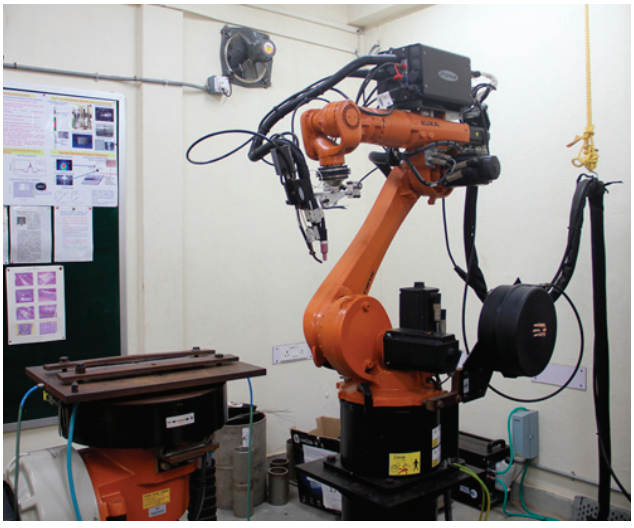

Figure 1: Robotic hot wire TIG welding machine at MJS

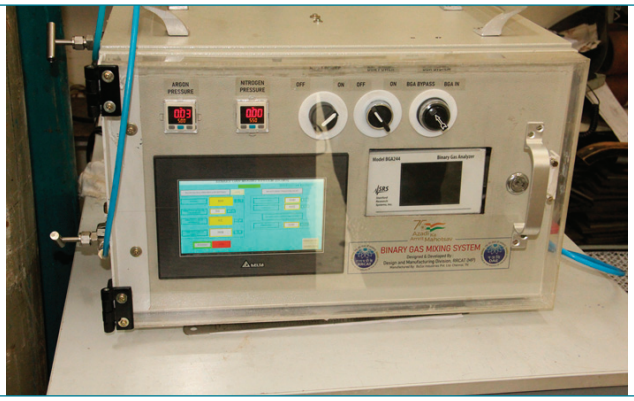

Figure 2: Image of precise binary gas mixing unit from RRCAT, Indore

Hence, N enhanced 316L(N) SS is being proposed as the structural material for the FBR components. However, there is no matching consumable available for joining high nitrogen 316L(N) SS till date.

Hence, a study on the properties of N enhanced 316L(N) SS weld joints containing different levels of N content in the weld metal are to be carried out to optimize the N content in the weld metal for the fabrication of components. Therefore, it was decided to introduce nitrogen in the weld metal through shielding gas using robotic TIG welding machine so that 316L(N) weld metals with different N contents can be produced. Hence, 316L(N) weld metals containing various levels of N in it were produced in laboratory scale and its properties were studied.

1. Preparation of nitrogen enhanced 316L(N) weld metal

Nitrogen containing 316L(N) SS weld metals were produced using robotic hot wire TIG welding facility available in Materials Joining Section (MJS) (Figure 1). A precise binary gas mixing unit produced by RRCAT, Indore (Figure 2), was used to mix calculated volume

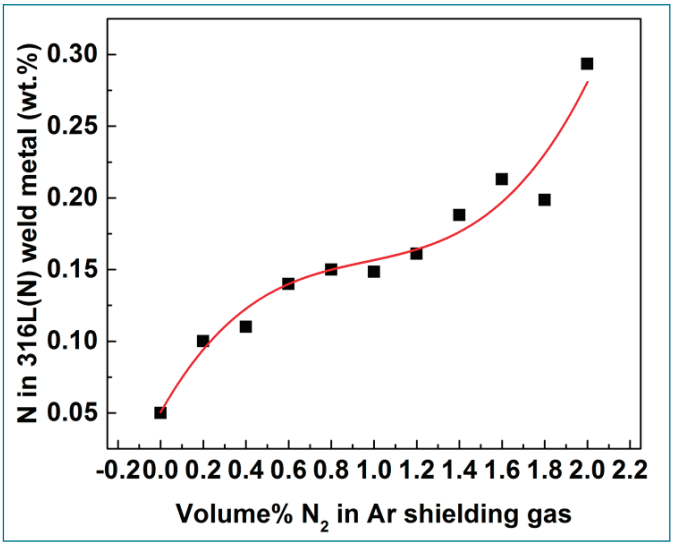

Figure 3: Plot showing relationship between the N2 gas mixed with Ar shielding gas and actual weld metal N content.

percent of N to the argon shielding gas (Ar) during welding to adjust the weld metal nitrogen content.

A base plate of 316L SS was chosen for the weld deposit trials. The chemical composition of 316L base plate is shown in Table.1.

ER 3I6L consumable was deposited on the base plate by adding different volume percent of N_2 to the Ar- shielding gas.

Table 1: Chemical composition in wt.%

	Cr	Ni	Mo	Mn	Si	C	Cu	Fe
Base plate	19.4	12	2.0	2.1	0.4	0.03	0.75	Bal.
Filler wire	18.9	12.6	2.09	1.82	0.68	0.03	0.08	bal

The chemical composition of the ER 316(L) consumable is given in Table. 1. The weld deposits produced with various N additions were analyzed for its N content using Bruker's make ONH analyzer in the welding laboratory. The optimized ratios of Ar + N_2 for the desired N content in the weld metal are arrived after several trials. The volume percent of N_2 gas added to the Ar shielding gas is plotted against the measured N content in the 316L(N) weld deposit and shown in Figure 3.

Thus, 316L(N) weld joints with weld metals containing five different levels of N were prepared using the welding parameters shown in Table.2. The N content in the weld metals are given in Table 3.

Actual weld joints with desired N contents in 316L(N) weld metals were prepared using 316L SS base plates and by choosing the (Ar + N_2) mixing ratios from the graph shown in Figure 3.

Table 2: Welding parameters used for weld pad fabrication using robotic hot wire TIG facility.

Current	180 A
Polarity	DCEN
Voltage	16.6
Travel speed	60 mm/min
Shielding gas	Ar + N_2
Shielding gas flow rate	10 liter/minute
Position	1G

Table 3: 316L(N) SS weld joints containing 316L(N) weld metal of various N content.

Vol.% N_2 in shielding gas	N content in 316L(N) weld metal (wt.%)
0	0.05
0.1	0.08
0.2	0.10
0.4	0.11
0.8	0.14

Table 4: Ferrite Number measured and predicted for N containing 316L(N) weld metal.

	N content in 316L(N) weld metal (wt.%)	Ferrite Number (Ferritescope)	Ferrite Number WRC-92.
1	0.05	5	4
2	0.08	4	3
3	0.10	3	2
4	0.11	2.5	1
5	0.14	0.2	0

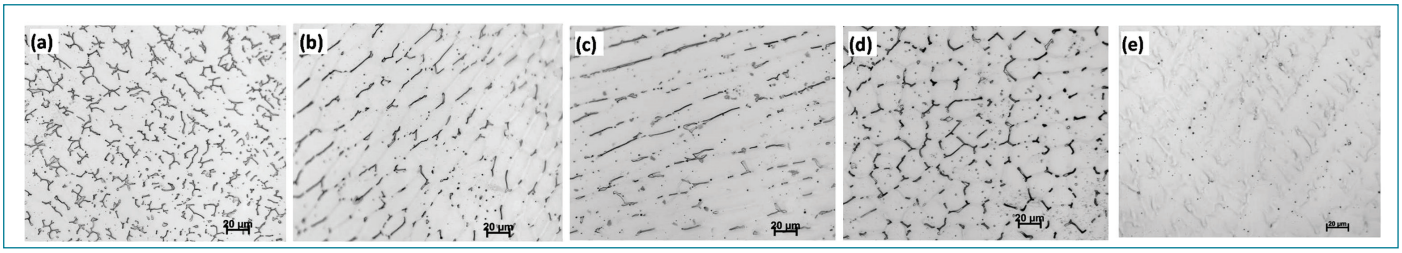

Figure 4: Photomicrographs of 316L(N) weld metal containing (a) 0.05 wt.% N (b) 0.08 wt.% N (c) 0.10 wt.% N (d) 0.11 wt.% N (e) 0.14 wt.% N.

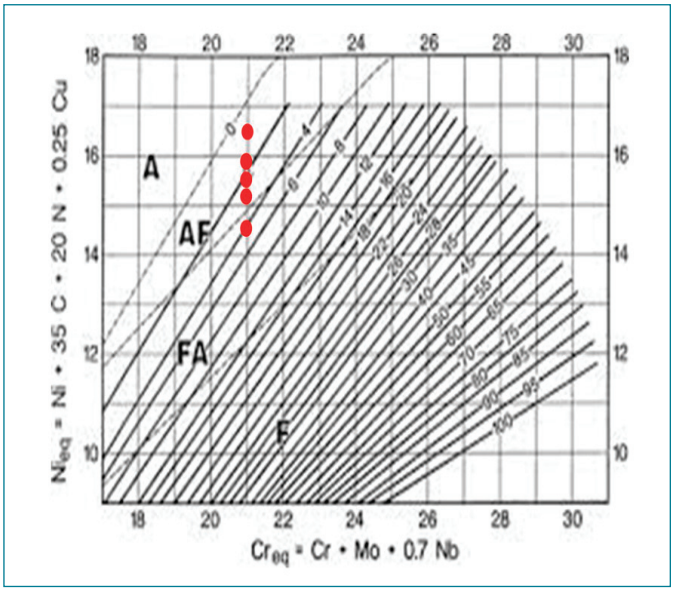

Figure 5: WRC-92 constitution diagram showing 316L(N) weld metal micro constituents containing different N wt.%.

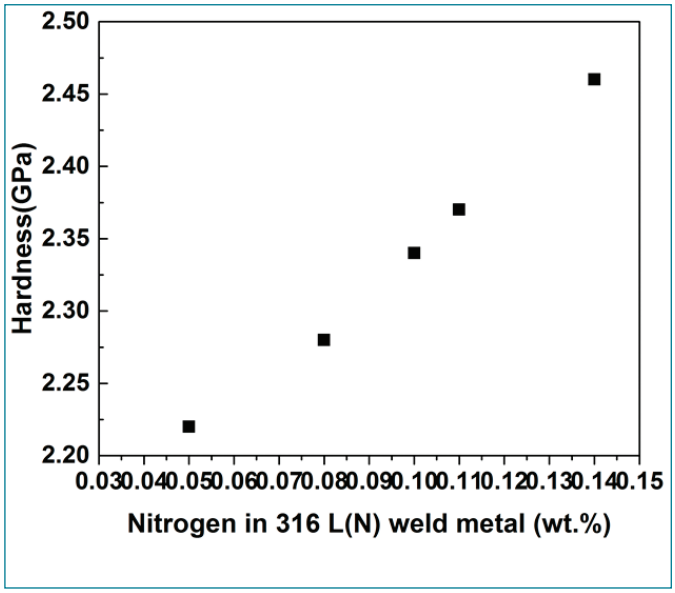

Figure 6:Hardness values of nitrogen added 316L(N) weld metal using nano indentation tests at 100 mN load.

2. Effect of N on microstructures of 316L(N) weld metals

Figure 4 shows the microstructures of 316L(N) weld metal containing different levels of nitrogen. The microstructures of 316L(N) weld metal containing nitrogen up to 0.11 wt.% shows presence of delta-ferrite in the weld metal. Beyond 0.11 wt.% N, the microstructure shows predominantly austenitic dendrites and some inclusions. From the photomicrographs, it is apparent that there are significant differences in the microstructure of the weld metals containing different N level. This is possibly due to change in mode of solidification from primary ferrite to primary austenite with increasing N content in the weld metal. The effect of N on 316L(N) weld metal microstructure is depicted on the WRC-92 diagram as shown in Figure 5. WRC-92 diagram is an empirical diagram used to predict austenitic weld metal microstructure based on chemical composition of the weld metal. For constitution of the WRC-92 diagram, the chemical composition of the weld metal is categorized into ferrite stabilizers and austenite stabilizers. The ferrite stabilizing elements are taken for Cr equivalent calculation, X- axis. The austenite stabilizing elements are taken for Ni-equivalent calculation, Y-axis.

From Figure 5, it is clearly discernable that the mode of solidification changes from primary ferrite to primary austenite with increasing N content in the weld metal. The microstructures of the N containing weld metals shown in the Figure 4 is consistent with the microstructure predicted by the WRC -92 diagram.

The ferrite numbers (FN) measured using ferritescope and that predicted using WRC-92 diagram is given in Table. 4. The measured ferrite numbers are almost in agreement with the predicted values.

3. Room temperature nano- indentation studies on the 316L(N) weld metals

To study the effect of N on the mechanical properties of 316L(N) weld metal, nano- indentation technique was used. The nano-indentation studies were carried out using 100 mN load at room temperature. The indentations were made at the core of the dendrites as the aim is to study the effect of nitrogen present in solid solution in the austenite matrix on the hardness.

The hardness values obtained for the N enhanced weld metals are given in Figure 6. The figure shows that the hardness of the austenite matrix has significantly increased with increase in the N content of the weld metal.

This report highlights that 316L(N) weld metal containing different levels of N using the precise binary gas mixing unit during robotic hot wire TIG welding process were successfully prepared at materials joining section (MJS). Subsequently, 316L(N) SS weld joints were prepared with N enhanced 316L(N) weld metal. The preliminary investigations showed that the N enhancement in the weld metal has pronounced effect on the solidification mode of the weld metal, microstructure and hardness. Evaluation of mechanical and corrosion properties of these weld metals are in progress to qualify the joint.

Corresponding Author:
Dr. M. Divya, MMG

Young Researcher's Forum

Dr. Madhura. B completed her Ph. D in Engineering Science from HBNI in 2022 and her work focused on thermal barrier coatings for pyrochemical reprocessing applications. Madhura B received her B.Sc and M.Sc degree in Materials Science from Mangalore University, Karnataka, and M.Sc. (Engg.) in 2017 from HBNI. She joined in Corrosion Science & Technology Division, MMG, IGCAR, Kalpakkam as JRF in March 2015 under a dual degree Integrated Ph. D program. Currently, she is working as Post-Doctoral Fellow at University West, Trollhättan, Sweden, Focusing on Environmental Barrier Coatings for aerospace applications. She has published 8 papers in peer-reviewed international journals, with a few being co-authored. Dr Madhura is a recipient of JB Joshi Endowment Innovation Award – 2023, HBNI.

Development of Interlayer Coatings on Graphite with Top Y_2O_3 Coating for Pyrochemical Reprocessing Applications

The spent metallic nuclear fuel from the future fast breeder reactors (FBR's) in India will be processed through a non-aqueous reprocessing route, namely pyrochemical reprocessing. The major unit operations in pyro reprocessing, namely, cathode and injection casting processors, employ high-density graphite (HDG) materials as crucible materials. Due to its outstanding refractoriness and thermal shock resistance, HDG is the best-chosen crucible material for temperatures ranging from 773-1773 K in highly corrosive molten salt (e.g., eutectic LiCl-KCl) and U-Pu-Zr (uranium, plutonium, and zirconium) environment. However, the spontaneous oxidation of

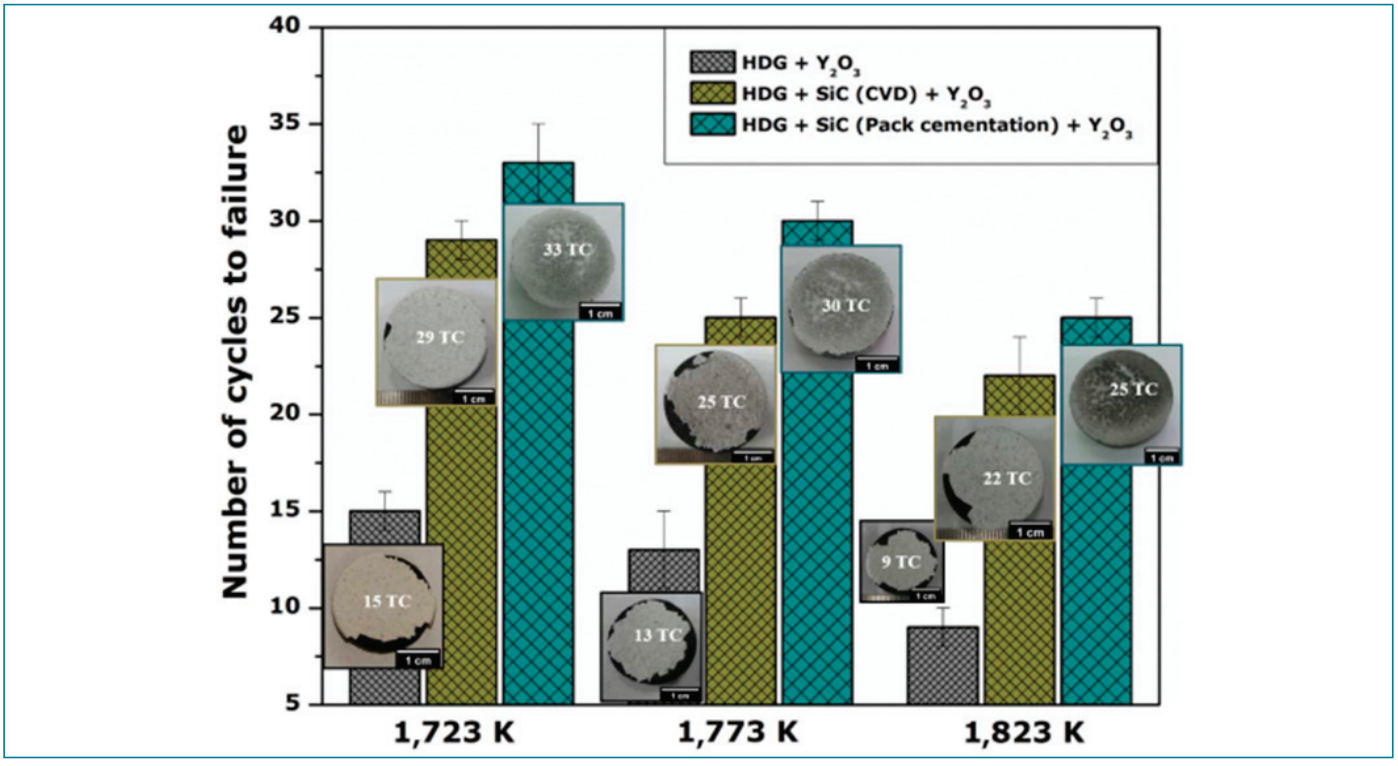

Figure 1: Bar chart representing the number of thermal cycles to failure at 1,723, 1,773, and 1,823 K with photographs corresponding to failed samples.

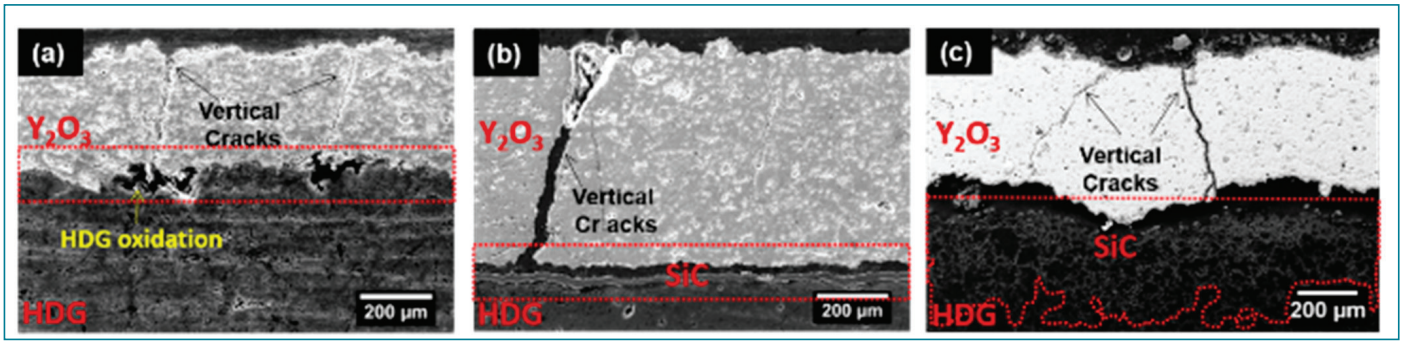

Figure 2: SEM cross-sectional morphology of Y_2O_3 coating failure during the thermal cycle at 1,823 K with and without interlayer: (a) over bare HDG substrate; (b) silicon carbide interlayer by CVD; (c)with silicon carbide interlayer by pack cementation

graphite materials beyond 773 K in the presence of oxygen and the feasibility of forming metal carbides and intercalation compounds restrict the usage of bare HDG crucible in reprocessing applications. Due to its thermal/chemical stability atmospheric plasma sprayed (APS) Y_2O_3 coatings on HDG are widely used in cathode processing and injection casting operations. However, on repeated U-Zr melting cycles, delamination of plasma-sprayed Y_2O_3 coating can occur due to thermal expansion mismatch, sintering-induced coating densification, and thermal fatigue failure which leads to carbon contamination of U-Zr ingot. Hence a suitable interlayer coating is highly essential for better performance of the Y_2O_3 coated HDG substrate.

In general, refractory carbides, borides, and nitrides interlayer's on graphite substrates are the better choice for high-temperature applications.

In this context, the study has been focused on addressing the following major things (1) investigation on the understanding of the plasma spray parameters for attaining optimum porosity in characteristic lamellae Y_2O_3 coating by APS technique for enhanced thermal stability and mechanical integrity up to 1773 K; (2) to develop viable interlayers (carbide and boride) with intermediate coefficients of thermal expansion between top Y_2O_3 coating and HDG substrate using commercial deposition processes (CVD and Pack cementation); (3) the life assessment of these coatings for U-Zr melting application and demonstrating coating failure mechanisms with and without interlayer. Finally, U interaction studies have been carried out by performing U melting cycles in coated crucible samples in an induction melting system installed in an inert atmosphere glove box.

Y_2O_3 coating is sprayed on HDG at 25, 30 and 35 kW plasma powers while retaining other spray parameters in the optimized window. The spray watch diagnostic system has been utilized to measure in-flight particle temperature and velocity with varying plasma spray power at a fixed stand-off distance. The phase stability, mechanical property, and failure mechanisms correlated to microstructure for three variants are analyzed for pristine and thermal cycle tested coatings. The plasma spray power 30 kW was found to perform well, resulting in sufficient melting of Y_2O_3 feedstock powder resulting in a pancake disc-shaped splat on impact. However, cracking/delamination failure of Y_2O_3 coating on HDG due to thermal expansion mismatch was found to be inevitable after $\sim$ 10 thermal cycles at 1773 K, necessitating a suitable interlayer alleviating mismatch stress (Figure 1).

Towards interlayer development, the SiC coating by Chemical Vapor Deposition technique using methyl trichlorosilane (MTS-99%) and hydrogen as a reactive precursor at 1293 K for 30 h was attempted. CVD-grown SiC coatings with uniform thickness and dense morphology exhibited excellent oxidation protection for HDG substrates due to its ability to form passive vitreous silica (SiO_2) layer with minimum oxygen permeability. SiC coating with a smooth surface finish demanded additional surface preparation methods prior to Y_2O_3 coating by APS. The two-fold enhancement in thermal cycle life (22 thermal cycles at 1773 K) found in the presence of SiC interlayer was attributed to the minimization of thermal expansion mismatch. However, the spallation of Y_2O_3 coating during the thermal cycle ascribed to weak interfacial bonding between Y_2O_3 and CVD-grown SiC necessitated the study of alternative interlayer development processes (Figure 2).

Further, a simple and low-cost pack cementation chemical route to develop a diffused and infiltrated thick SiC interlayer over HDG followed by top Y_2O_3 coating by APS was attempted. The U melting cycles performed with pack cemented SiC interlayer was found to withstand up to 10 U melting cycles without failure or delamination of Y_2O_3 coating (Figure 3).

However, at temperatures beyond 1773 K, active oxidation by breakdown or decomposition of the SiC layer was found to be more pronounced, thus demanding ultrahigh-temperature composite ceramics as interlayer for further enhancing the durability and operational limits.

The investigation on the performance and durability of Y_2O_3 coating

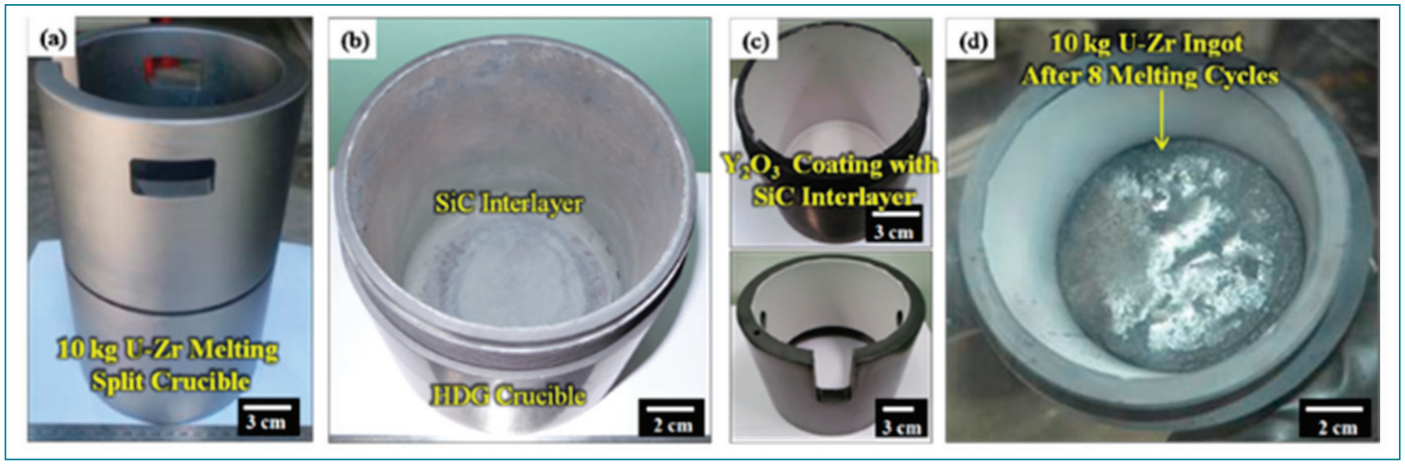

Figure 3: Digital images of (a) 10 kg U-Zr melting HDG split crucibles (OD 150 mm, ID 120 mm, and an internal depth of 220 mm), (b) SiC interlayer at the inner wall, (c) APS Y_2O_3 top coating with SiC interlaid HDG split crucible and (d) U-Zr ingot in coated crucibles after 8 melting cycles

with SiC-ZrB2 ultra-high-temperature ceramic composite interlayer by pack cementation method on HDG was attempted. Adding ZrB2 to SiC promotes the formation of ultra-high-temperature oxidation-resistant ternary silicate-based glasses ($ZrSiO_4$), which are more stable and offer superior protection over monolithic SiO_2. It was found that the presence of SiC-ZrB_2 interlayer of intermediate CTE value minimized the magnitude of differential mismatch-induced tensile stress, consequently enhancing the life of Y_2O_3 coating up to 35 cycles. The findings of this work provide systematic data and information on the development of suitable and durable inter-layers (SiC and SiC-ZrB_2) on HDG for Y_2O_3 deposition for pyrochemical reprocessing applications.

With interlayer the enhanced thermal cycle durability of Y_2O_3 coating up to 22 -25 cycles (Fig. 1) and U melting cycles withstand up to 10 U melting cycles without Y_2O_3 coating failure (Figure 3). In the application front, these interlayers impede and restrict the carbon contamination in U ingot from HDG crucible; otherwise, possible thorough defects and cracks in the Y_2O_3 top coat by the formation of passive oxidation products viz., SiO_2, ZrO_2 and $ZrSiO_4$ phases are evident. The systematic understanding of APS Y_2O_3 coating failure mechanism at elevated temperature and introduction of suitable interlayer's thereby enhanced thermal cycle life; navigate the design process for Y_2O_3 coating used in U melting crucibles were successfully demonstrated (Figure 3).

Interactions with Academia

April 10-11, 2023

IGCAR- IIT Hyderabad interactive meeting

A delegation of 13 faculty from IIT Hyderabad visited IGCAR during 10-11 April 2023 to explore collaborative projects with IGCAR. The team visited various research facilities of IGCAR and based on the interactions, broad areas for collaboration were identified.

Reported by
John Philip, MMG

Incubation Agreement Signed with Private Industry for Oil Level Measurement System

April 25, 2023

A collaborative incubation agreement, as per DAE Incubation Policy (2021), has been signed on April 25, 2023 between DAE Incubation Centre-IGCAR and a Chennai based private industry for EIG, IGCAR's "Oil Level Measurement System". Inset (Left): Signing of the incubation agreement; Inset (Right): Presentation on the technology by Ms. N. Malathi, EIG prior to signing the agreement on 25.04.2023.

Technology Incubation Activities: A collaborative incubation agreement, as per DAE Incubation Policy (2021), has been signed on 25. April. 2023 between DAE Incubation Centre-IGCAR and a Chennai based private industry for IGCAR's "Oil Level Measurement System" for EIG, IGCAR. This incubation programme is expected to accelerate development of this IGCAR technology from its current technology readiness level (TRL) of '7' to TRL '8' or '9', with value-additions suitable for commercialisation, during the incubation period of ~14 months.

Reported by
Dr. N. Subramanian
Safety, Quality & Resource Management Group

Summer Training Program in Physics and Chemistry (STIPAC-2023)

May 30, 2023

Releasing of books by Dr. V. Ravindran, Director, IMSc, Chennai during the inaugural function of Summer Training Program in Physics and Chemistry (STIPAC-2023)

Materials Science Group (MSG) has prided itself in its consistent and exemplary work on radiation effects on solids. The very first IGCAR report RRC 1 (1973) titled "Radiation damage in Reactor materials" carrying an article by Dr. G. Venkataraman on "Voids in irradiated metals and alloys" followed by a series of reports on defect studies in different reactor materials have given a great impetus to the Radiation damage and Defect studies program at MSG. Keeping this background of almost five decades of research work in the defect studies, the role of defects in Condensed Matter at MSG was reviewed in a Two day internal meeting held during 3-4 November 2022. This meeting had talks by experts on various aspects of defects in materials which are being currently investigated in MSG. These talks were compiled in to a book titled "Role of Defects in Condensed Matter: Vistas from Materials Science Group" bearing ISBN No. 978-81-955370-1-3. The book comprised of 11 chapters describing the scientific contributions by the colleagues of MSG, was released on 30th May 2023 at the Vikram Sarabhai Auditorium by Dr. V. Ravindran, Director, IMSc, Chennai during the inaugural function of Summer Training Program in Physics and Chemistry (STIPAC-2023).

Reported by
Dr. R. Govindaraj
Materials Science Group

Inauguration of Met-Ocean Data Buoy with Radiation Monitor

June 02, 2023

Figure 1: Inauguration of Data Buoy by Director, IGCAR

Figure 2: Data Buoy

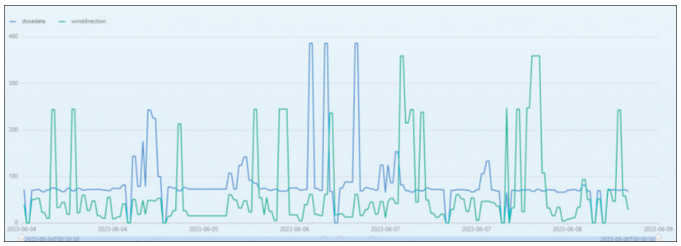

Figure 3: Real-time data

As part of Emergency preparedness program, Safety, Quality & Resource Management Group (SQRMG) has deployed a Met-Ocean Data Buoy with Radiation monitor about 1-km from the coast in the coastal waters of Kalpakkam site. The Radiation Buoy was inaugurated by Director, IGCAR on 2nd June 2023. The Buoy is designed with a number of meteorological and ocean sensors [anemometer, air humidity & temperature sensor, pressure, rainfall sensor, Surface CT sensor, current meter, wave meter], mechanical and mooring components and sinker weight with the technical guidance from National Institute of Ocean Technology (NIOT), Chennai. The IGCAR developed radiation monitor is integrated with the onboard CPU. The buoy provides environmental parameters of winds, temperature, humidity, wave height, ocean current, sea water conductivity and temperature, and radiation dose rate data from the sea sector to the Online Decision Support System ONERS operational at Kalpakkam site for the management of Off-site emergencies. The real-time data is transmitted using GPRS to the server at IGCAR. Presently there are 27 radiation monitors distributed in nine land sectors connected to ONERS. The data buoy would enhance the existing monitoring radiation monitoring network and provides data from the sea sector for effective tracking of radioactive plume during emergency scenario when the plume moves to the sea-area. The buoy data will also be useful for modelling of radioactivity dispersion in coastal waters, extreme wind and wave height measurement during cyclonic conditions for disaster management besides environmental studies.

Reported by
Dr. C. Venkata Srinivas
Safety, Quality & Resource Management Group

Best Paper/Poster Award

• Dr. B. Sasi received the Best Poster award for the paper titled, "Development of eddy current sensors for quality control of nuclear components", presented in the XV Triennial &III international Conference on the theme: Women in Science & Technology, held during 11th-13th June 2023 at IWSA-HQ, Navi Mumbai.

• Srujana M*, B. B. Lahiri, John Philip received the Best Poster award of International Conference on Functional materials for Future Technology (IC-FMFT 2023) held during April 19-21, 2023 for the poster titled "Viscosity dependent studies on the magnetic fluid hyperthermia efficiency of magnetite nanoparticles coated with a bio-compatible polymer"

Bio-diversity @ DAE Campus, Kalpakkam

Red-Whiskered Bulbul is a very rarely seen bird in Kalpakkam complex. It has brown upperparts, white underparts with a broken blackish necklace on breast. It has a beautiful glossy black spilled crest, red patch behind eyes and white patches on lower ear coverts. Both male and female look similar.

Published by Scientific Information Resource Division, SQ&RMG, IGCAR, Kalpakkam-603102